Size Dependence of the Surface Plasmon Resonance Damping in Metal Nanospheres

ARTICLE *in* JOURNAL OF PHYSICAL CHEMISTRY LETTERS · OCTOBER 2010

Impact Factor: 7.46 · DOI: 10.1021/jz1009136

THE JOURNAL OF PHYSICAL CHEMISTRY Letters

pubs.acs.org/JPCL

Size Dependence of the Surface Plasmon Resonance Damping in Metal Nanospheres

Jean Lermé,* Hatim Baida, Christophe Bonnet, Michel Broyer, Emmanuel Cottancin, Aurélien Crut, Paolo Maioli, Natalia Del Fatti, Fabrice Vallée, and Michel Pellarin

Laboratoire de Spectrométrie Ionique et Moléculaire (UMR 5579), Université de Lyon, Université Lyon I, CNRS, Bât. A. Kastler, 43 B[ld] du 11 Novembre 1918, F-69622 Villeurbanne Cedex, France

ABSTRACT The impact of quantum confinement on the width of the surface plasmon resonance of a metal nanoparticle is theoretically investigated in a model system formed by a silver nanosphere in different environments. Calculations are performed using the time-dependent local density approximation (TDLDA) for nanoparticle diameters up to about 11 nm, permitting precise quantification of the surface plasmon broadening due to size reduction. As expected, this is found to be inversely proportional to the particle diameter, but with an amplitude strongly depending on the environment (increasing by a factor of 4 when changing from vacuum to alumina). This is ascribed to the fact that damping is governed by the electronic surface spill-out (inherent in any quantum model) and thus strongly depends on the surface profile of the confining potential, that is, on the particle surface conditions.

SECTION Nanoparticles and Nanostructures

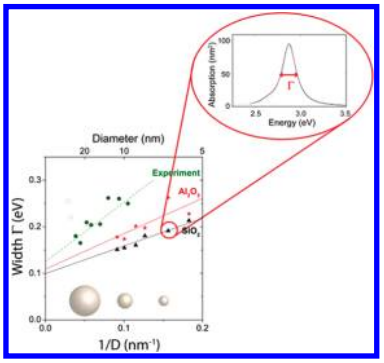

The optical properties of noble metal nanoparticles have attracted a lot of interest during the past decade. This is motivated by the appearance of a strong resonance in their absorption and scattering spectra, the localized surface plasmon resonance (LSPR). The strong dependence of its wavelength on the particle size, shape, and environment has been extensively exploited to elaborate new materials with optical properties adapted to specific requirements.[1−8] A key parameter for many applications, for example nanosensing, nanolabeling, or surface-enhanced fluorescence and Raman spectroscopies, is the quality factor of the resonance. This is intrinsically limited by the homogeneous width of the LSPR, which reflects relaxation of the collective electron oscillation resonantly driven by the optical field.

The main relaxation mechanism is the radiative damping for large-size particles (diameters larger than a few tens of nanometers).[9,10] Scaling as the particle volume, it becomes negligible for small sizes (below about 20 nm), where dephasing effects dominate. The damping of the collective electron motion then takes place with excitation of single electron−hole pairs in the conduction band (Landau damping), assisted by the intrinsic electron scattering processes, that is, electron−electron, −ion, or −defect scattering (a similar mechanism also takes place when the LSPR overlaps the interband transitions, as in gold or copper, with excitations promoting d band electrons into the conduction band). When the particle size becomes smaller than the electron mean-free path set by the intrinsic electron scattering, electron scattering off the surface has to be taken into account. This additional mechanism, frequently introduced classically using a billiard approach,[11−15] actually reflects quantum confinement of the conduction electrons in the particle. It constitutes an intrinsic limit to the LSPR width in small particles and is thus a limiting factor in the possible size reduction for many applications.

Though global increase of the LSPR width with size reduction has been experimentally observed in ensemble measurements, the reported data show a large dispersion of the amplitude of the surface effect, together with a large dependence on the environment (referred to as chemical damping).[16,17] This has probably to be ascribed to a large inhomogeneous broadening of the LSPR due to dispersions of the size, shape, and local environment of the particles.

Using single metal nanoparticle spectroscopies,[18−29] the size impact on the width of the LSPR can now be precisely addressed on a single size-characterized nanoparticle, as recently reported in model systems (silver nanospheres with a silica shell).[29] Quantitative interpretation of these data requires precise quantum mechanical calculations of the surface-induced broadening effects going beyond the quantum box model.[30−32] In this model, the conduction electrons are confined in a flat-bottom potential well of infinite depth, and the dielectric function of the particle is then computed by taking into account dipolar transitions between the confined quantized electronic states. This leads to a bulk-like Drude-type expression, with an additional surface contribution to the electronic scattering rate, which reflects in the LSPR width, Γ

$$\Gamma(R) = \Gamma_0 + g\frac{v_F}{R} \quad (1)$$

Received Date: July 5, 2010
Accepted Date: September 14, 2010
Published on Web Date: September 17, 2010

DOI: 10.1021/jz1009136 | J. Phys. Chem. Lett. 2010, 1, 2922–2928

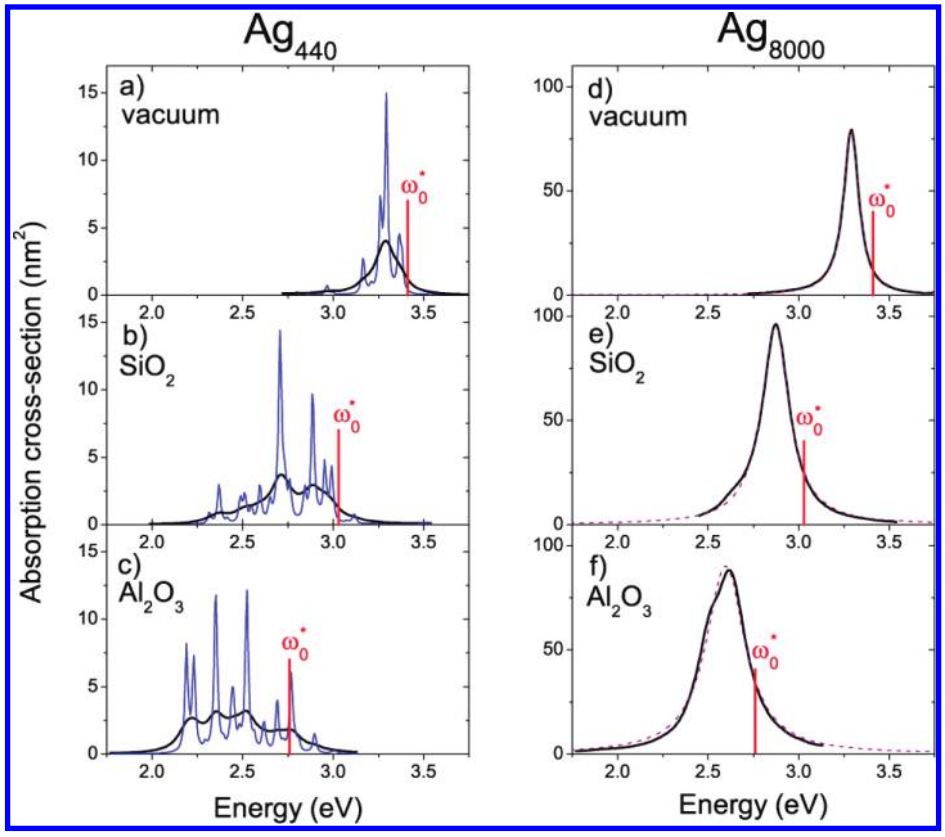

Figure 1. Absorption cross sections of Ag_{440} ($D \approx 2.4$ nm) clusters (a) in vacuum or (b) embedded in SiO_2 or (c) Al_2O_3, computed using a jellium model with intrinsic broadening parameters of $\delta = 10$ and 60 meV in eq 7 (light-colored and black curves, respectively). The vertical bars indicate the classical plasmon resonance ω_0^* for each matrix. (d−f) Same as (a−c) for Ag_{8000} ($D \approx 6.4$ nm) clusters, with $\delta = 60$ meV only, together with a fit assuming a Lorentzian shape (dashed curves).

where Γ_0 is the contribution due to the intrinsic electron scattering, v_F the Fermi velocity, and R the radius of the spherical particle. However, these calculations involve various approximations at the origin of the dispersion of the computed values of the parameter g.[31,32]

In this Letter, we theoretically analyze the impact of confinement on the width of the LSPR in metal nanoparticles using a more realistic confinement potential. In connection with experimental studies, computation was performed for silver spheres over a large enough size range (diameter D from 3 to 11 nm) to precisely quantify the size evolution of the LSPR width, that is, g in eq 1. For the sizes of the nanospheres of interest here, calculations can be performed by modeling the matrix-embedded particle as an electron gas (the conduction electrons) in interaction with a ionic background described by a spherical homogeneous jellium (density ρ_{0+}) of diameter D (the discrete ionic lattice is thus disregarded).[33,34] The confinement potential is computed self-consistently in the Kohn−Sham (KS) formulation of the density functional theory (DFT).[33−35] It is worthwhile recalling that in the KS-DFT formalism, the self-consistent KS potential energy, $V_{eff}[\mathbf{r},\rho_0]$, expresses as the sum of three contributions, namely the interaction with the background, $V_{jel}(\mathbf{r})$ (see hereafter), the Coulomb interaction with the electron gas, $V_{ee}[\mathbf{r},\rho_0]$, and the exchange-correlation contribution $V_{xc}[\mathbf{r},\rho_0]$. The occupied (which determine the ground-state electron density $\rho_0(\mathbf{r})$) and unoccupied single-electron KS orbitals and energies are then determined, and the optical response is calculated in the TDLDA formalism.[33−35] The screening effects and the optical response of the inner dielectric background (that includes the core electrons) and of the non-absorbing matrix are taken into account via their dielectric functions $\varepsilon_1(\omega)$ and $\varepsilon_2(\omega)$, respectively.[36,37] In silver, the interband absorption threshold lies at about 4 eV ($\varepsilon_1(\omega)$ is real in the LSPR spectral range); therefore, the resonance width is not affected by the broadening mediated by interband absorption (case of gold and copper). Details of the theoretical modeling can be found in refs 36 and 37; therefore, only the equations relevant for the discussion are reported (atomic units are used: $q = \hbar = m = 4\pi\varepsilon_0 = 1$).

In the presence of an applied external field $E_0 e^{-i\omega t}\mathbf{e}_z$ of frequency ω (to which corresponds the electron potential energy $V_{ext}(\mathbf{r},\omega) = zE_0$ in the nonretarded or quasi-static limit), the particle is polarized (total dipole $\mathbf{p}(t) = \alpha(\omega)E_0 e^{-i\omega t}\mathbf{e}_z$, with $\alpha(\omega) = \alpha_c(\omega) + \alpha_e(\omega)$). The absorption cross section $\sigma(\omega)$ is computed from the imaginary part of the total polarizability $\alpha(\omega)$ according to

$$\sigma(\omega) = \frac{4\pi\omega}{c\sqrt{\varepsilon_2(\omega)}}\,\mathrm{Im}[\alpha_c(\omega) + \alpha_e(\omega)] \qquad (2)$$

The first term of the polarizability, $\alpha_c(\omega)$, corresponds to the polarization charges at the jellium/matrix interface that are directly induced by the applied field $\mathbf{E}_0$.[36,37] It does not

DOI: 10.1021/jz1009136 | J. Phys. Chem. Lett. 2010, 1, 2922–2928

contribute to the absorption in the LSPR spectral range ($\varepsilon_1(\omega)$ and $\varepsilon_2(\omega)$ are real). To these induced polarization charges corresponds the potential energy $V_{\alpha c}(\mathbf{r},\omega)$. The second term, $\alpha_e(\omega)$, is the polarizability that is associated with the induced oscillating conduction electron charge density (total density $\rho_0(\mathbf{r}) + \delta\rho(\omega,\mathbf{r})e^{-i\omega t}$). $\delta\rho(\omega,\mathbf{r})$ and $\alpha_e(\omega)$ can be expressed as[36,37]

$$\delta\rho(\mathbf{r},\omega) = \int \chi(\mathbf{r},\mathbf{r}',\omega)V_{ext}'(\mathbf{r}',\omega)\,d\mathbf{r}' \quad (3)$$

$$\alpha_e(\omega) = -\frac{1}{E_0^2}\int \delta\rho(\mathbf{r},\omega)V_{ext}'(\mathbf{r},\omega)\,d\mathbf{r} \quad (4)$$

where $V'_{ext}(\mathbf{r},\omega) = V_{ext}(\mathbf{r},\omega) + V_{\alpha_c}(\mathbf{r},\omega)$ and $\chi(\mathbf{r},\mathbf{r}',\omega)$ is the nonlocal many-body correlation function. According to the TDLDA formalism, the response of the interacting conduction electrons is calculated as in the independent particle case, provided that the induced variation of the ground-state (index 0) mean-field Kohn−Sham potential energy $V_{eff}[\mathbf{r},\rho_0]$, that is

$$\delta V_{eff}[\mathbf{r},\omega] = \int \left[\frac{\delta V_{eff}[\mathbf{r},\rho]}{\delta\rho}\right]_{\rho_0} \delta\rho(\mathbf{r}',\omega)\,d\mathbf{r}' \quad (5)$$

is added to $V'_{ext}(\mathbf{r},\omega)$ in eq 3. The induced electron density $\delta\rho(\mathbf{r},\omega)$ is therefore the solution of an implicit equation, permitting $\chi(\mathbf{r},\mathbf{r}',\omega)$ to be expressed, through an integral equation, in terms of the independent electron correlation function $\chi^0(\mathbf{r},\mathbf{r}',\omega)$. $\chi^0(\mathbf{r},\mathbf{r}',\omega)$ can be written in terms of retarded single-particle Green's functions $G(\mathbf{r},\mathbf{r}',\omega)$ of the ground-state KS Hamiltonian, namely

$$\chi^0(\mathbf{r},\mathbf{r}',\omega) = \sum_i [\varphi_i^*(\mathbf{r})\varphi_i(\mathbf{r}')G(\mathbf{r},\mathbf{r}',E_i+\omega) + \varphi_i(\mathbf{r})\varphi_i^*(\mathbf{r}')G^*(\mathbf{r},\mathbf{r}',E_i-\omega)] \quad (6)$$

with

$$G(\mathbf{r},\mathbf{r}',E) = \langle\mathbf{r}|[H-E-i\delta]^{-1}|\mathbf{r}'\rangle \quad (7)$$

where H is the single-particle KS ground-state Hamiltonian. In eq 6, the index i runs over the occupied ground-state KS wave functions φ_i of energies E_i (a $T = 0$ K temperature is assumed). The parameter δ introduces phenomenologically line broadening effects that are not included here. It corresponds to attributing an intrinsic width of about 2δ to each transition between confined electronic states. For negligible surface effects, that is, for large sizes, this translates into an intrinsic LSPR width that can be identified with the bulk contribution $\hbar\Gamma_0$ (eq 1). The value of $2\delta = 120$ meV, consistent with experimental determination,[29] has been used in most calculations.

The main term that will rule the computed quantum broadening effect is the screened electron−jellium potential energy $V_{jel}(\mathbf{r})$ entering the effective ground-state KS potential energy $V_{eff}[\mathbf{r},\rho_0]$. In the presence of polarizable media (the ionic cores and the matrix), the bare Coulomb interaction between an electron and the jellium sphere has to be modified to take into account screening effects from both media. Simple classical calculations lead to the following effective interaction energy (in atomic unit)

$$V_{jel}(r<R) = \frac{Q_+}{2\varepsilon_1(0)R}\left[\frac{r^2}{R^2} - 1 - 2\frac{\varepsilon_1(0)}{\varepsilon_2(0)}\right] = \frac{1}{2}\frac{\omega_0^2}{\varepsilon_1(0)}\left[r^2 - \left[1+2\frac{\varepsilon_1(0)}{\varepsilon_2(0)}\right]R^2\right] \quad (8)$$

$$V_{jel}(r>R) = -\frac{Q_+}{\varepsilon_2(0)r} \quad (9)$$

where Q_+ is the total jellium charge (in atomic units) and $\omega_0 = \omega_P/3^{1/2}$ ($\hbar\omega_P = 8.98$ eV is the plasma energy in bulk silver).

The computed absorption cross section spectra of a silver particle in silica ($\varepsilon_2 \approx 2.16$), alumina ($\varepsilon_2 \approx 3.2$), and vacuum ($\varepsilon_2 = 1$) are shown in Figure 1. For very small sizes, the LSPR exhibits a matrix-dependent fragmentation due to the large energy spacing of the quantized electronic levels involved in photon absorption (this fragmentation fades away when increasing the intrinsic broadening of the individual transitions, that is, δ in eq 7). The matrix dependence results from the induced change of the confining potential and, consequently, of the single electron state spectrum (see Figure 1a−c). For larger sizes, the LSPR line evolves toward a quasi-Lorentzian structureless line shape (see Figure 1d−f), as expected from classical calculations using Mie theory.

The center of the structured plasmon band is noticeably red-shifted relative to the LSPR frequency ω_0^*, computed using the classical approach. This shift has been discussed before and is related to the amount of electrons spilling out from the particle (spill-out effect;[33] see Figure 2). This effect is thus more pronounced for a large refractive index matrix (larger screening) and for small sizes for which surface effects predominate. As expected, for large sizes, typically more than 1000 atoms ($D \geq 3$ nm), the quantum calculated LSPR frequency converges toward ω_0^* (see Figure 1d−f).

The computed structure exhibits a large size and matrix-dependent broadening that eventually converges toward the intrinsic one, which is about 2δ for very large sizes. Like the LSPR red shift, this LSPR broadening is also directly related to the density of the spill-out electrons, that is, the density of electrons experiencing the surface profile of the confining potential. It thus strongly depends on the details of this potential, a sensitivity which is at the origin of the matrix dependence. The increased screening by the matrix, that is, the increase of its refractive index, softens the edge of the effective confining potential V_{eff}, concomitantly increasing the spill-out effect (see Figure 2). Except for very small sizes, involving very few occupied energy levels, the surface profiles of V_{eff} and of the electron density are quasi-size-independent. As any surface-mediated effect, this contribution to the LSPR broadening thus decreases when increasing the particle size.

For quantifying the LSPR broadening and its size dependence, a least-squares Lorentzian curve fitting of the computed spectra has been performed for particles larger than about 3 nm (in the range of 832 to 40 000 atoms), for which such a profile can be used (see Figure 1d−f). For the smallest

DOI: 10.1021/jz1009136 | J. Phys. Chem. Lett. 2010, 1, 2922–2928

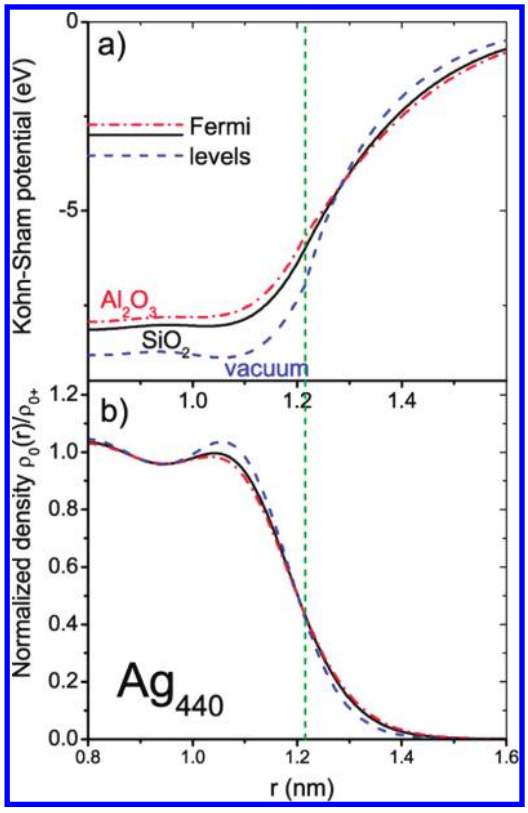

Figure 2. Effective Kohn−Sham potentials (a) and normalized ground-state densities (b) for Ag_{440} ($D \approx 2.4$ nm) in vacuum, SiO_2, and Al_2O_3 (dashed, solid, and dot−dashed curves, respectively). The short horizontal lines in (a) indicate the Fermi levels for each matrix and the vertical line the particle radius R (jellium edge).

sizes, fragmentation of the LSPR band leads to large variations of the estimated full width at half-maximum Γ with the particle size. A smoother dependence is obtained for the largest sizes ($N \geq 5000$ or $D \geq 5.5$ nm), Γ recovering its expected linear dependence on the inverse particle radius (see eq 1 and Figure 3). By increasing the size, Γ converges to the LSPR width Γ_0 yielded by Mie theory in the dipolar approximation ($\Gamma_0 \approx 2\delta/(1 + \omega_0^{*3}/2\omega_P^2[\partial\varepsilon_1/\partial\omega]_{\omega_0^*})$, leading, for $\delta = 60$ meV, to $\Gamma_0 \approx 0.104$ eV, 0.110 eV, and 0.086 eV for SiO_2, Al_2O_3, and vacuum, respectively. From a linear fit of the Γ values determined in this large size range and taking into account the asymptotic width Γ_0, g values of 0.09 (vacuum), 0.32 (SiO_2), and 0.42 (Al_2O_3) were obtained, independently of the δ value used in the calculations. The relative change of the g value is consistent with that of the matrix indexes.

The computed g parameter is consistent with recent experimental results obtained by investigating the LSPR spectrum of single silver nanospheres coated with silica.[29] The experimental data, also reported in Figure 3, show a LSPR broadening for particles smaller than about 20 nm, with an overall experimental value of $g_{exp} \approx 0.7 \pm 0.1$ (the large increase of the LSPR width measured for large sizes, $D > 25$ nm, is due to the radiative damping,[8−10] concomitant with retardation effects not included here). This value is about two times larger than the theoretical value computed in this work $g \approx 0.32$ (confinement contribution only), suggesting additional

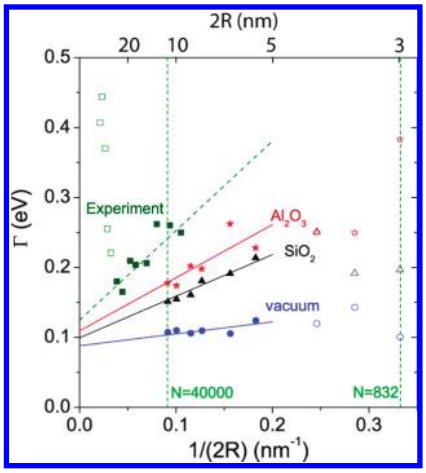

Figure 3. Computed dependence of the LSPR full width at half-maximum Γ on the inverse of the diameter of a silver sphere in vacuum (circles), SiO_2 (triangles), or Al_2O_3 (stars) extracted from a Lorentzian shape fit of the computed absorption cross section spectra, with $\delta = 60$ meV in eq 7. The full lines are linear fits of the six largest size data (solid symbols) and the asymptotic value (see text). The squares are experimental data[29] (empty square symbols correspond to large sizes influenced by multipolar effects), and the corresponding line is a fit using eq 1 with $\hbar\Gamma_0 = 0.125$ eV and $g = 0.7$. The experimental data are the experimental LSPR bandwidths (full width at half-maximum) determined through the procedure described in ref 29.

contribution in this size range. Including the size dependence of the intrinsic damping (Γ_0), that is, mostly of the electron−phonon scattering, a corrected experimental value of $g \approx 0.4 \pm 0.1$ for the confinement contribution was then estimated.[29] This is in better agreement with the theoretical value of 0.32 estimated in this work. Additional surface effects at the interface of the silver core−silica shell of the chemically synthesized nanoparticles (chemical damping), surface defects, and the corrugation of the potential well can introduce additional size dependencies and might be at the origin of the residual discrepancy.

The sensitivity of the LSPR surface broadening, that is, of g, on the surrounding matrix is directly related to its sensitivity to the details of the surface profile of the confining potential $V_{eff}[\mathbf{r},\rho_0]$. This reflects the fact that the profile is governed by the potential due to the ionic background ($V_{jel}(\mathbf{r})$, eqs 8 and 9), especially the Coulombic part experienced by the electrons which spill out. This can be illustrated by calculating the optical absorption of cationic particles M_N^{q+} within the standard jellium model ($\varepsilon_1(\omega) = \varepsilon_2(\omega) = 1$ are assumed in the following illustrative examples). In cationic particles, the electron spill-out tail is slightly reduced as compared to that for neutral particles, essentially localizing the excess positive charges at the surface, as expected from classical electrodynamics (see Figure 4a).[38] Although the differences in the overall electronic densities are small, particle charging leads to significant modifications of the optical spectra, which show a concomitant reduction of the LSPR width and an increase of the resonance frequency (see Figure 4b). They approach the classical values of $\Gamma_0 = 2\delta$ and $\omega_0 = \omega_P/3^{1/2}$ when increasing the charge $q+$, reflecting the reduction of surface effects, that is, reducing deviation from the large particle regime. This clearly stresses that the surface-induced plasmon damping is

DOI: 10.1021/jz1009136 | J. Phys. Chem. Lett. 2010, 1, 2922–2928

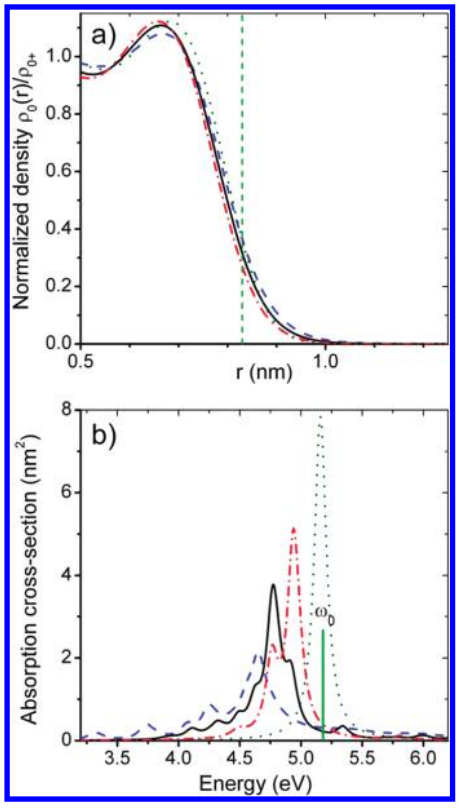

Figure 4. Normalized ground-state densities (a) and absorption cross sections (b) for Ag_{138} (dashed line), Ag_{138}^{4+} (solid line), and Ag_{138}^{8+} (dot−dashed line) clusters computed using the standard jellium model with the electron−jellium potential given by eqs 8 and 9 (with $\varepsilon_{1,2}(0) = 1$) and for Ag_{138} assuming a fully harmonic potential ($V_{har}(r)$; see text; dotted curves), with $\delta = 60$ meV in eq 7. The vertical dashed line in (a) is the particle radius R, and the short vertical bar in (b) indicates the classical plasmon resonance energy $\hbar\omega_0$. Note that the results reported here are not directly comparable with the absorption properties of real silver particles in vacuum since the screening effects from the core electrons are disregarded.

mainly determined by the density of electrons experiencing the nonharmonic part of the electron−background interaction (eqs 8 and 9).

This is further supported by computing the optical response of a model spherical system, assuming a harmonic electron−background potential energy over the whole space ($V_{har}(r) = (1/2)\omega_0^2 r^2 + C$, instead of $V_{jel}(r)$, in eqs 8 and 9, for any r). Physically, this corresponds to a positive ionic background fully embedding all of the electrons, that is, extending over a size exceeding the electronic density tail, so that the Coulombic interaction (eq 9) beyond the surface is not experienced by the electrons. As compared to the standard jellium potential for an R radius particle (eqs 8 and 9), this leads to a KS confinement potential with a much steeper surface variation. The corresponding absorption spectrum consists of a single Lorentzian line at almost the classical plasmon frequency ω_0, with the expected intrinsic width $\Gamma_0 = 2\delta$ (see Figure 4b; the very small frequency shift is probably due to the approximate local exchange-correlation functional that is used). This absence of significant red shift and additional broadening is in stark contrast with the results of the standard jellium model. Actually, the self-consistent KS potential obtained with $V_{har}(r)$ is more similar to that used in the quantum box model[30−32] (as compared to the one obtained with $V_{jel}(r)$), though no surface effect is predicted here. This clearly points out that the LSPR shift and broadening are ruled by the electronic density tail experiencing the nonparabolic part of the electron−background potential close to the surface (eq 9). This behavior is consistent with that reported for finite electron systems confined in semiconductor nanostructures. Actually, it has been shown that the collective oscillatory motion (which corresponds to the center-of-mass coordinate) separates from the intrinsic individual excitations when the electron−background interaction is purely harmonic.[39−41] This decoupling can be analytically shown for a model system with no background dielectric effects ($\varepsilon_{1,2}(\omega) = 1$). If the electron−background interaction energy is purely harmonic (i.e., $V_{e-b}(\mathbf{r}) = \omega_a^2 r^2/2$), the Hamiltonian representing N_e interacting electrons can be separated into two commuting parts describing the motion of their center of mass and the individual motions (involving $N_e - 1$ independent vector coordinates), respectively. The collective oscillation (center-of-mass motion) is thus decoupled from individual ones, is undamped if other processes are neglected, and occurs at the frequency ω_a.[39−41]

The next logical extension of the theoretical approach would be to take into account the granular atomistic structure of the background (giving rise to the electron−ion (phonon) scattering contribution), but at this moment, this challenge does not seem realizable over the large size range investigated due to prohibitive computational times (loss of the spherical symmetry). In the frame of jellium-type background modeling, calculations have been carried out involving a lower jellium density at the surface. The results, as well as the analysis of the expected impact in the case of rough or faceted particles, show that, in all cases, the surface profile of the self-consistent confinement potential is slightly softened, and the electronic spillout tail is enlarged, thus the LSPR damping and g factor in eq 1.

In conclusion, the evolution of the LSPR width in small silver nanospheres has been calculated within a quantum mechanical approach based on the TDLDA formalism. In the large size regime (larger than about 5 nm), the LSPR shows a Lorentzian-shaped profile with a width linearly increasing with the inverse particle size, characteristic of quantum confinement (or surface)-induced broadening. This additional broadening was shown to be ruled by surface effects, that is, the amount of electrons experiencing the nonharmonic part of the electron−ionic core interaction potential close to the particle surface. It has a similar physical origin as the quantum-confinement-induced red shift of the LSPR in small nanoparticles. The amplitude of this surface-induced broadening is shown to largely depend on features characterizing the nanoparticle surface and environment, that is, the vacuum or nature of the matrix, and thus on the shape of the confining potential. These features were not taken into account in previous models (quantum box models) where an infinite depth potential well was assumed, masking details of the electron−surface interaction potential and, in particular, the influence of the matrix. Though different in nature, this

DOI: 10.1021/jz1009136 | J. Phys. Chem. Lett. 2010, 1, 2922–2928

sensitivity is in qualitative agreement with the large LSPR broadening observed experimentally when changing the chemical condition of the nanoparticle surface, for example, by bonding surfactant molecules.

In the case of SiO_2-embedded silver nanospheres, the results are consistent with experimental studies when taking into account other possible sources of size dependencies. Though similar surface-induced effects are expected in other noble metal nanoparticles (such as gold or copper), involvement of interband-induced broadening makes data analysis and comparison of experimental and theoretical results more complex (the frequency shift with size of the LSPR changes the overlap with interband transitions and thus the interband damping contribution). Similar experiments on single metal nanoparticles coated with matrixes of different nature would be very interesting to investigate the size dependencies computed here.

AUTHOR INFORMATION

Corresponding Author:

*To whom correspondence should be addressed. Tel: +33 472431137. Fax: +33 472431507. E-mail: lerme@lasim.univ-lyon1.fr.

ACKNOWLEDGMENT M.B. and N.D.F. thank the Institut Universitaire de France (IUF).

REFERENCES

(1) Stewart, M. E.; Anderton, C. R.; Thompson, L. B.; Maria, J.; Gray, S. K.; Rogers, J. A.; Nuzzo, R. G. Nanostructured Plasmonic Sensors. *Chem. Rev.* **2008,** *108*, 494–521.

(2) Kühn, S.; Hakanson, U.; Rogobete, L.; Sandoghdar, V. Enhancement of Single-Molecule Fluorescence Using a Gold Nanoparticle as an Optical Nanoantenna. *Phys. Rev. Lett.* **2006,** *97*, 017402.

(3) Lal, S.; Grady, N. K.; Kundu, J.; Levin, C. S.; Lassiter, J. B.; Halas, N. J. Tailoring Plasmonic Substrates for Surface Enhanced Spectroscopies. *Chem. Soc. Rev.* **2008,** *37*, 898–911.

(4) Wilson, R. The Use of Gold Nanoparticles in Diagnostics and Detection. *Chem. Soc. Rev.* **2008,** *37*, 2028–2045.

(5) Jaint, P. K.; El-Sayed, I. H.; El-Sayed, M. A. Au Nanoparticles Target Cancer. *Nanotoday* **2007,** *2*, 18–29.

(6) Kelly, K. L; Coronado, E.; Zhao, L. L.; Schatz, G. C. The Optical Properties of Metal Nanoparticles: The Influence of Size, Shape, and Dielectric Environment. *J. Phys. Chem. B* **2003,** *107*, 668–677.

(7) Liz-Marzan, L. M. Nanometals: Formation and Color. *Mater. Today* **2004,** *7*, 26–31.

(8) Kreibig, U.; Vollmer, M. *Optical Properties of Metal Clusters*; Springer: Berlin, Germany, 1995.

(9) Teperik, T. V.; Popov, V. V.; Garcia de Abajo, F. Radiative Decay of Plasmons in a Metallic Nanoshell. *J. Phys. Rev. B* **2004,** *69*, 155402.

(10) Dahmen, C.; Schmidt, B.; von Plessen, G. Radiation Damping in Metal Nanoparticle Pairs. *Nano Lett.* **2007,** *7*, 318–322.

(11) Kreibig, U.; Fragstein, C. V. The Limitation of Electron Mean Free Path in Small Silver Particles. *Z. Phys.* **1969,** *224*, 307–323.

(12) Kreibig, U. Electronic Properties of Small Silver Particles: The Optical Constants and Their Temperature Dependence. *J. Phys. F: Met. Phys.* **1974,** *4*, 999–1014.

(13) Coronado, E. A.; Schatz, G. C. Surface Plasmon Broadening for Arbitrary Shape Nanoparticles: A Geometrical Probability Approach. *J. Chem. Phys.* **2003,** *119*, 3926–3934.

(14) Liu, M.; Guyot-Sionnest, Ph. Synthesis and Optical Characterization of Au/Ag Core/Shell Nanorods. *J. Phys. Chem. B* **2004,** *108*, 5882–5888.

(15) Moroz, A. Electron Mean Free Path in a Spherical Geometry. *J. Phys. Chem. C* **2008,** *112*, 10641–10652.

(16) Persson, B. N. J. Polarizability of Small Spherical Metal Particles: Influence of the Matrix Environment. *Surf. Sci.* **1992,** *281*, 153.

(17) Hövel, H.; Fritz, S.; Hilger, A.; Kreibig, U.; Vollmer, M. Width of Cluster Plasmon Resonances: Bulk Dielectric Functions and Chemical Interface Damping. *Phys. Rev. B* **1993,** *48*, 18178–18188.

(18) Klar, T.; Perner, M.; Grosse, S.; von Plessen, G.; Spirkl, W.; Feldmann, J. Surface-Plasmon Resonances in Single Metallic Nanoparticles. *Phys. Rev. Lett.* **1998,** *80*, 4249–4252.

(19) Sönnichsen, C.; Geier, S.; Hecker, N. E.; von Plessen, G.; Feldmann, J.; Ditlbacher, H.; Lamprecht, B.; Krenn, J. R.; Aussenegg, F. R.; Chan, V. Z. H.; et al. Spectroscopy of Single Metallic Nanoparticles Using Total Internal Reflection Microscopy. *Appl. Phys. Lett.* **2000,** *77*, 2949–2951.

(20) Mock, J. J.; Barbic, M.; Smith, D. R.; Schultz, D. A.; Schultz, S. Shape Effects in Plasmon Resonance of Individual Silver Nanoparticles. *J. Chem. Phys.* **2002,** *116*, 6755–6759.

(21) Sönnichsen, C.; Franzl, T.; Wilk, T.; von Plessen, G.; Feldmann, J. Drastic Reduction of Plasmon Damping in Gold Nanorods. *Phys. Rev. Lett.* **2002,** *88*, 077402.

(22) Lindfors, K.; Kalkbrenner, T.; Stoller, P.; Sandoghdar, V. Detection and Spectroscopy of Gold Nanoparticles Using Supercontinuum White Light Confocal Microscopy. *Phys. Rev. Lett.* **2004,** *93*, 037401.

(23) Berciaud, S.; Cognet, L.; Lounis, B. Photothermal Absorption Spectroscopy of Individual Semiconductor Nanocrystals. *Nano Lett.* **2005,** *5*, 2160–2163.

(24) Arbouet, A.; Christofilos, D.; Del Fatti, N.; Vallée, F.; Huntzinger, J. R.; Arnaud, L.; Billaud, P.; Broyer, M. Direct Measurement of the Single-Metal-Cluster Optical Absorption. *Phys. Rev. Lett.* **2004,** *93*, 127401.

(25) Muskens, O. L.; Billaud, P.; Broyer, M.; Del Fatti, N.; Vallée, F. Optical Extinction Spectrum of a Single Metal Nanoparticle: Quantitative Characterization of a Particle and Its Local Environment. *Phys. Rev. B* **2008,** *78*, 205410.

(26) Billaud, P.; Marhaba, S.; Cottancin, E.; Arnaud, L.; Bachelier, G.; Bonnet, C.; Del Fatti, N.; Lermé, J.; Vallée, F.; Vialle, J. L.; et al. Correlation between the Extinction Spectrum of a Single Metal Nanoparticle and its Electron Microscopy Image. *J. Phys. Chem. C* **2008,** *112*, 978–982.

(27) Hu, M.; Novo, C.; Funston, A.; Wang, H.; Staleva, H.; Zou, S.; Mulvaney, P.; Xia, Y.; Hartland, G. V. J. Dark-Field Microscopy Studies of Single Metal Nanoparticles: Understanding the Factors That Influence the Linewidth of the Localized Surface Plasmon Resonance. *Mater. Chem.* **2008,** *18*, 1949–1960.

(28) Billaud, P.; Marhaba, S.; Grillet, N.; Cottancin, E.; Bonnet, C.; Lermé, J.; Vialle, J. L.; Broyer, M.; Pellarin, M. Absolute Optical Extinction Measurements of Single Nano-Objects by Spatial Modulation Spectroscopy Using a White Lamp. *Rev. Sci. Instrum.* **2010,** *81*, 043101.

(29) Baida, H.; Billaud, P.; Marhaba, S.; Christofilos, D.; Cottancin, E.; Crut, A.; Lermé, J.; Maioli, P.; Pellarin, M.; Broyer, M.; et al. Quantitative Determination of the Size Dependence of Surface Plasmon Resonance Damping in Single Ag@SiO_2 Nanoparticles. *Nano Lett.* **2009,** *9*, 3463–3469.

(30) Kawabata, A.; Kubo, R. Electronic Properties of Fine Metallic Particles. II. Plasma Resonance Absorption. *J. Phys. Soc. Jpn.* **1966,** *21*, 1765–1722.
(31) Ruppin, R.; Yatom, Y. Size and Shape Effects on the Broadening of the Plasma Resonance Absorption in Metals. *Phys. Status Solidi* **1976,** *74*, 647–654.
(32) Barma, M.; Subrahmanyam, V. Optical Absorption in Small Metal Particles. *J. Phys.: Condens. Matter* **1989,** *1*, 7681.
(33) Brack, M. The Physics of Simple Metal Clusters: Self-Consistent Jellium Model and Semiclassical Approaches. *Rev. Mod. Phys.* **1993,** *65*, 677–731.
(34) Ekardt, W. Size-Dependent Photoabsorption and Photoemission of Small Metal Particles. *Phys. Rev. B* **1985,** *31*, 6360–6370.
(35) Zangwill, A.; Soven, P. Density-Functional Approach to Local-Field Effects in Finite Systems: Photoabsoroption in the Rare Gases. *Phys. Rev. A* **1980,** *21*, 1561–1572.
(36) Lermé, J.; Palpant, B.; Cottancin, E.; Pellarin, M.; Prével, B.; Vialle, J. L.; Broyer, M. Quantum Extension of Mie's Theory in the Dipolar Approximation. *Phys. Rev. B* **1999,** *60*, 16151–16156.
(37) Lermé, J. Introduction of Quantum Finite-Size Effects in the Mie's Theory for a Multilayered Metal Sphere in the Dipolar Approximation: Application to Free and Matrix-Embedded Noble Metal Clusters. *Eur. Phys. J. D* **2000,** *10*, 265–277.
(38) As the charge of the M_N^{q+} cluster is increased, large changes in the Friedel oscillations inside of the cluster are usually observed in $\rho_0(\mathbf{r})$. These changes are mainly correlated with the changes of the occupied (n,l) level set in the ground state. However, the average inner electron density remains equal to ρ_{0+} far from the surface, and the increase of the total cluster charge is more reflected through a systematic reduction of the electronic spillout tail.
(39) Brey, L.; Johnson, N. F.; Halperin, B. I. Optical and Magneto-Optical Absorption in Parabolic Quantum Wells. *Phys. Rev. B* **1989,** *40*, 10647–10649.
(40) Maksym, P. A.; Chakraborty, T. Quantum Dots in a Magnetic Field: Role of Electron−Electron Interactions. *Phy. Rev. Lett.* **1990,** *65*, 108–110.
(41) Dobson, J. F. Harmonic-Potential Theorem: Implications for Approximate Many-Body Theories. *Phys. Rev. Lett.* **1994,** *73*, 2244–2247.

DOI: 10.1021/jz1009136 | *J. Phys. Chem. Lett.* **2010,** *1*, 2922–2928